proceedings

MDPI

Proceedings

Structural Characterization of the Decomposition Product of Hexamethylenetetramine (HMTA) under Classical Duff Conditions. A Combined Theoretical and Spectroscopic Study †

Sebastián O. Simonetti [1,*], Teodoro S. Kaufman [1], Rodolfo Rasia [2], Ariel M. Sarotti [1] and Nicolás Grimblat [1,*]

[1] Instituto de Química Rosario (IQUIR, CONICET-UNR), Facultad de Ciencias Bioquímicas y Farmacéuticas—Universidad Nacional de Rosario, Suipacha 531, Rosario 2000, Argentina; simonetti@iquir-conicet.gov.ar; kaufman@iquir-conicet.gov.ar; sarotti@iquir-conicet.gov.ar; grimblat@iquir-conicet.gov.ar

[2] Instituto de Biología Molecular y Celular de Rosario, Consejo Nacional de Investigaciones Científicas y Tecnológicas, Universidad Nacional de Rosario, 2000 Rosario, Argentina; rasia@ibr-conicet.gov.ar

† Presented at the 24th International Electronic Conference on Synthetic Organic Chemistry, 15 November–15 December 2020; Available online: https://ecsoc-24.sciforum.net/.

Received: date; Accepted: date; Published: date

Abstract: In a joint DFT and spectroscopic study, we were able to elucidate the decomposition products of Hexamethylenetetramine (HMTA) under the conditions commonly employed for the Duff formylation (high temperature in acidic media). The combination of these techniques allowed us to unravel the structures of near-identical intermediates of the reaction. The results of this work will increase even further the fields where this amine plays an important role

Keywords: Hexamethylenetetramine; NMR study; density functional theory

1. Introduction

Hexamethylenetetramine (HMTA) is a widely known nitrogen heterocycle characterized by a cage-like structure reminiscing the adamantane motif. This versatile compound has an ample array of relevant scientific and technological applications (Scheme 1), and its metal complex-forming ability has been at the heart of multiple reports [1]. Recently, the use of HMTA in materials science has aroused extraordinary interest within the scientific community [2], since it proved to be an ideal component for the manufacture of ZnO microflowers, and different classes of nanomaterials [3].

On the other hand, HMTA is used for the production of phenol-formaldehyde polymers and acts as curing agent for traditional and advances phenolic resins [4]. Moreover, the recent synthesis of its carboxyborane derivative is a promising pharmacological application of this amine [5]. Furthermore, HMTA has astrophysical importance; being formed under deep space conditions, it becomes relevant to understand the interstellar ices [6]. Being such a valuable structure, it also sparked research on the functionalization of adamantanes [7] and adamantane-like structures containing nitrogen atoms [8]. In synthetic organic chemistry, HMTA is used in the obtention of benzaldehyde derivatives through the Duff formylation [9] or the Sommelet reaction [10]. Moreover, its derivatives like the HMTA.Br_2 complex are used in several synthetic applications under mild conditions [11]. Recently, the use of HMTA was further spread by its application as a ligand of different transformations [12].

These valuable uses of HMTA require a thorough understanding of its properties and characteristics, because this will prompt for the development of new applications and the

improvement of the performance of existing ones. Given our continued interest in natural products, we became attracted by the Duff formylation as a green alternative to install a formyl moiety. Recently, we studied the factors governing the regioselectivity of this reaction, where HMTA acts as the formylation agent. We found that the path proceeds via an intramolecular proton rearrangement instead of an intermolecular transformation, as previously postulated. Consequently, we aim to elucidate the intermediates of this amine under the classical reaction conditions (high temperature and acidic media) [13]. These conditions have also been used to prepare certain polymers, oxidizing mixtures, special surfaces and other materials [14]; hence, details on HMTA stability could also be useful in these fields.

In order to unveil structural and mechanistic details about the stability and reactivity of HMTA and its intermediates and to be able to distinguish among the possible intermediates, we employed an array of analytical and computational techniques in a synergistic way, including NMR experiments, chemometrics tools, and DFT studies.

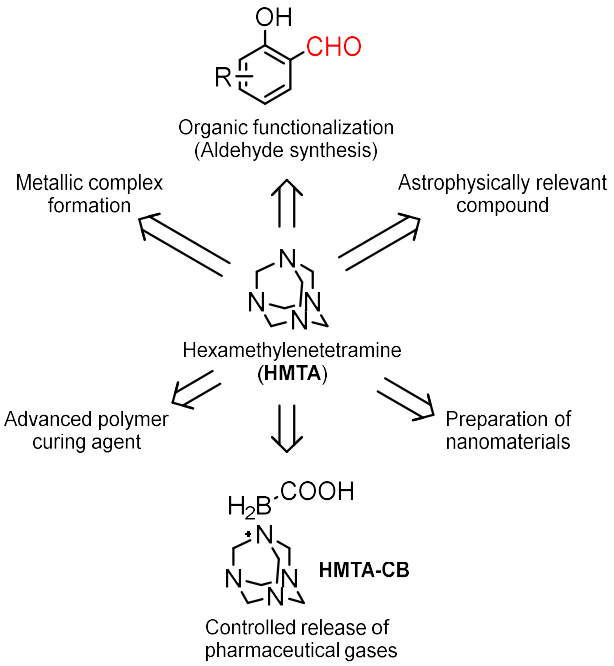

Scheme 1. Main applications of hexamethylenetetramine (**HMTA**) in several areas of chemistry.

2. Results and Discussion

To carry out the NMR spectroscopic analysis, HMTA was dissolved in AcOH-d_4 under ambient conditions, and spectra (Table 1) of the different nuclei involved (^{1}H, δ_H = 4.97 ppm (s); ^{13}C, δ_C = 71.6 ppm; and ^{15}N, δ_N = 38.7 ppm, entry 1) were recorded. Then, stepwise increments of 10 K were applied, acquiring ^{1}H NMR spectra at each step until the temperature reached 363 K. At this temperature (entry 2) we observed the first signs of a transformation, when the starting singlet began to be accompanied by a set of upfield and downfield signals. Among them, a pair of doublets (AB quartet) at δ_H = 4.60 and 4.71 ppm which correlated to a resonance at δ_C = 70.1 ppm, and a singlet at δ_H = 5.12 ppm related to the signal at δ_C = 80.7 ppm, can be highlighted. Figure 1 shows the different signals assigned to the proposed intermediates.

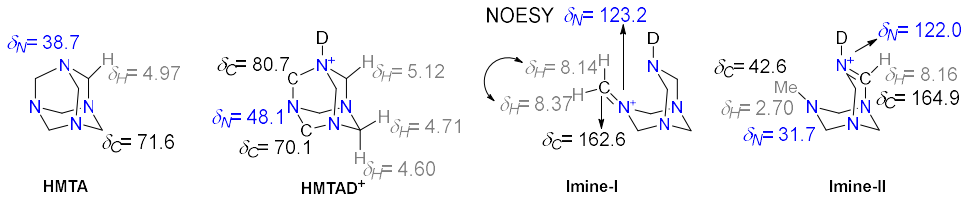

Figure 1. Observed diagnostic NMR signals for **HMTA**, the ring-opened imine (**Imine-II**) and the proposed intermediates **HMTAD**⁺ and **Imine-I** through the NMR experiments.

Interestingly, a similar pattern of signals was also observed in functionalized HMTA derivatives,[8] and could be related to a mono-deuterated ammonium intermediate species like **HMTAD**⁺. In this structure, the protons associated to the carbon attached to the positively charged nitrogen are magnetically equivalent and deshielded with regards to the non-protonated HMTA. The remaining hydrogens are diastereotopic, and are observed as an upfield doublet of doublets, where the most shielded signal corresponds to the most distant hydrogens from the charged heteroatom.

For more precise results, we carried out the same experiment employing labelled $^{15}N^{13}C$-HMTA. The ^{15}N NMR spectra at 343 K revealed a downfield shift to δ_N = 48.1 ppm, which was attributed to the protonated intermediate **HMTAD**⁺ by correlation by ^{15}N-^{1}H HMBC with the signals at δ_H = 5.12 ppm.

Table 1. Chemical shifts observed at the different temperatures. Multiplicities are displayed in parenthesis.

Temp.	Chemical Shifts (δ, ppm)		
(K)	^{1}H (δ)	^{13}C	^{15}N
298	4.97 (s)	71.6	38.7
343	4.60, 4.71 (AB quartet); 5.12 (s)	71.2; 80.5	48.1
348	8.14 (d), 8.37 (d)	162.6	123.2
353	2.70 (s), 8.16 (s)	42.8; 122.0	31.7
363	no new signals		

Based on previous observations, once the temperature of 343 K was reached, the system was heated to 348 K for 30 minutes. Under this condition, a new set of signals of increasing intensity became visible (entry 3), at δ_H = 8.14 ppm and δ_H = 8.37 ppm, being attributed to the formation of a new intermediate assigned as the iminium structure **imine-I**. A NOESY experiment revealed the correlation between both protons; furthermore, an HSQC experiment showed cross-peaks between each of these two protons and a carbon atom at δ_C = 162.6 ppm, which would confirm the proposed structure **imine I**. In the ^{15}N NMR spectrum at 348 K, a signal at δ_N = 123.2 ppm (iminium ion of **imine-I**) was observed, associated with the doublets at δ_H = 8.14 ppm and δ_H = 8.37 ppm.

Afterwards, the temperature was raised to 353 K (entry 4) and the appearance of an upfield singlet at δ_H = 2.70 ppm was observed in the ^{1}H NMR spectrum. This signal correlated with one at δ_C = 42.8 ppm in the ^{13}C NMR, being assigned to a *N*-methyl moiety. Additionally, another singlet was observed at δ_H = 8.16 ppm, that correlates with a peak at δ_C = 122.0 ppm; this led us to propose the **imine-II** as a potential intermediate. To verify this structure, the ^{15}N NMR spectrum was examined. This revealed a signal at δ_N = 31.7 ppm, which correlated with the *N*-methyl moiety and another at δ_N = 123.5 ppm which belongs to an iminium system, confirming the structure of the proposed intermediate.

To achieve a better understanding about the stability of the proposed intermediaries and the abundances of the most representative signals, each one was analysed. The employed procedures with each intermediate are represented in the Figure 2: *a*-A temperature ramp from 303 K to 363 K; *b*- an isothermic period of 90 minutes at 363 K, recording a ^{1}H spectra every 3 minutes; and *c*- an additional isothermic period of 6 h at 363 K, taking ^{1}H spectra every hour.

First, the peak intensity of native HMTA (δ_H = 4.92 ppm) was studied. It was observed that at 70 °C the peak began to decrease concomitant with the visibilization of additional signals. After 90 minutes at 363 K, a 50% decrease of the corresponding peak-area was observed, and after 6 hours almost 90% of the signal intensity had disappeared, giving rise to the proposed intermediates [15].

Analysis of the signals of the intermediaries proved to be challenging, since the proposed structures have ^{1}H NMR spectral signals very similar to each other, turning difficult the study of their relative abundance. An unambiguous signal was the one at δ_H = 2.66 ppm, attributed to the methyl moiety of the elucidated intermediate **imine-II**. When its abundance was examined, it was found to be rather low in the initial stages, while its presence became more pronounced over time (363 K for 90 minutes). Finally, in the 6-hour experiment, it was observed that the abundance of this signal, which reflects the prevalence of intermediate **imine-II**, remained constant after approximately two hours.

To study the intermediate **imine-I**, the modification of the peak intensity in the iminium region (8.00 to 8.60 ppm) was studied. There, a chemometrics approach involving a MCR-ALS analysis was applied, using the signal of the residual acidic proton of acetic acid (AcO**H**, δ = 2.00 ppm) as reference. This analysis showed that the variance of the iminium system is significantly explained (99.5%) by the presence of only two components, which were assigned to the intermediates **imine-I** and **imine-II**. It was also observed that the pattern of one of them shows a behaviour compatible with that of the methyl group previously described. Moreover, when the behavior of **imine-I** was analyzed, it was observed that its abundance peaks at 343 K, and then it begins to decline, presumably giving rise to the final intermediate **imine-II**. On the other hand, the peak deconvolution shows that at 363 K, the abundance of the signals attributable to the intermediate **imine-I** is much lower than those present for the intermediate **imine-II**; this is consistent with the disappearance of the cross-peaks observed in the NOESY spectrum. This trend was maintained in the 6 hours experiment.

Finally, these data were used to scrutinize the behaviour of the **HMTAD**$^+$ intermediate. Fortunately, applying the MCR-ALS algorithm to the signals in the region of δ = 4.75 ppm with acetic acid as a reference, it was observed that the variance of the system can be explained by only three components and that the signals of two of them are coincident with those suggested for **imine-I** and **imine-II**, respectively. Additionally, it was observed that the abundance of **HMTAD**$^+$ is lower than **imine-II**, but higher than **imine-I**.

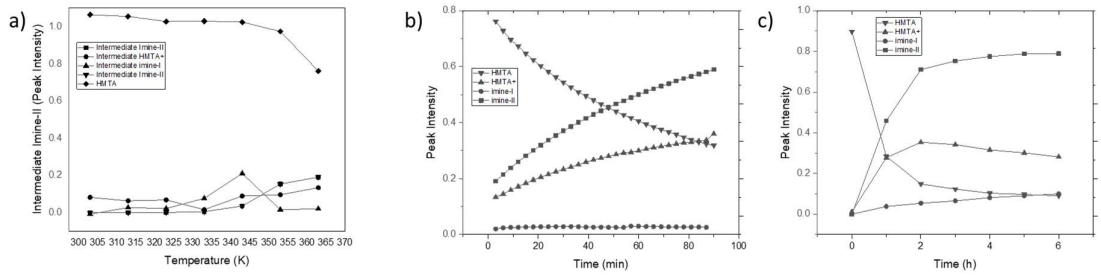

Figure 2. Peak-area Intensity of **HMTA** and the proposed intermediates in representative signals (**HMTAD**$^+$, **imine-I** and **imine-II**) under different conditions: (**a**) at a 30–90 °C ramp; (**b**) at 90 °C for 90 minutes and (**c**) at 90 °C for 6 hours.

According to the results, it can be conjectured that under the conditions of high temperature and acidic medium, the final product is one which has a methyl in its structure, attributable to **imine-II**. The intermediates **imine-I** (with an external iminium moiety) and **HMTAH**$^+$ seem to have low abundance and eventually short half-lifes under the reaction conditions, irreversibly forming **imine-II**.

Based on the NMR signal observation and interpretation, as well as signal analysis via MCR-ALS, we can propose the mechanistic evolution of HMTA towards the **imine-II** as shown in Scheme 2. In this proposal, the first stage of the multistep process entails the protonation of **HMTA** to afford the intermediate **HMTAH**$^+$ thanks to its good hydrogen bond acceptor characteristics. It has been

shown that simple mono-phenols form adducts having phenol:HMTA ratios of 1:1 or 2:1, where HMTA acts as either a mono- or a bis- hydrogen bond acceptor and it has even been found the heterocycle to act as a triple H-bond acceptor [16]. Interestingly enough, carboxylic acids were found to co-crystallize with HMTA, affording solids featuring 1–4 hydrogen bonds to the heterocycle [17]. However, it has been shown that the HMTA molecule only allows itself to be protonated once, being the only stable protonated compound [18].

The next step involved in the mechanism consists in the opening of **HMTAH**$^+$, to afford the Mannich base **Imine-I**. This transformation, which includes the concomitant formation of methylene minimum cations like **Imine-I**, was used in several synthetic methodologies, with HMTA and other aza-adamantanes as starting materials [19] According to the spectra, this transformation, which is likely triggered by protonation of the heterocycle by the solvent, is irreversible. Finally, at the highest recorded temperature (363 K), this intermediate could give place to **imine-II** through a 1,5-[H]-shift. This rearrangement, which involves two nitrogen atoms, is not uncommon and can be carried out thermally or with the use of Lewis acids [20].

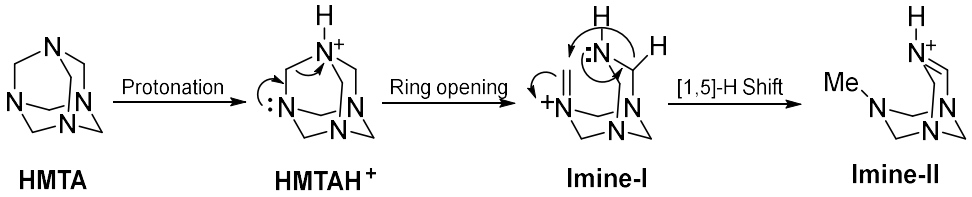

Scheme 2. Mechanistic proposal of the decomposition of HMTA in AcOH at high temperature.

To confirm this mechanistic proposal and understand the stability of the intermediates, an exhaustive DFT study was carried out employing the SMD(AcOH)/M062X/6.311+G(d,p) level of theory. The initial ring-opening step of **HMTAH**$^+$ towards the **imine-I** has an activation barrier of $\Delta G^{\neq}$ = 22.14 kcal mol^{-1}. This **TS**$_{\text{HMTAH+}}$, which corresponds to the opening of **HMTAH**$^+$, showed a C-N bond length of 2.40 Å, with a Wiberg index of 0.145. This gives rise to the **imine-I** with an energy of ΔG= 3.68 kcal mol^{-1}. The subsequent [1,5]-H shift towards **imine-II** has a $\Delta G^{\neq}$ = 37.02 kcal mol^{-1}. In the case of **TS**$_{\text{imine-I}}$, NBO calculations showed that the C_{α}-H bond length is 1.24 Å and the Wiberg index is 0.613, whereas for the C_{imine}-H bond, the length is 1.50 Å and the Wiberg index is 0.311.

The final intermediate **imine-II** shows to be 10.67 kcal mol^{-1} more stable than the proposed intermediate Mannich base **imine-I** (-6.99 kcal mol^{-1} overall). While the energy required for this proposed mechanism is achievable at the studied temperatures, it serves as an indicator of the relative stability of both imine intermediates. Therefore, this DFT study suggests a favourable pathway towards the iminium species **imine-II** through **imine-I** and shows that the latter is irreversibly converted into **imine-II**. A possible alternative is that at this temperature, the intermediates imine-I and HMTAH$^+$ are in equilibrium and irreversibly form **imine-II**.

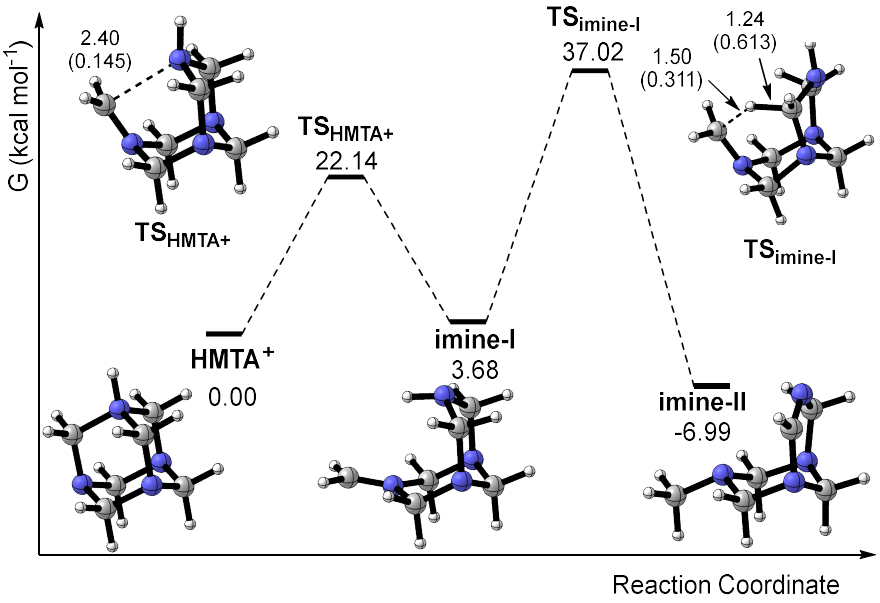

Scheme 3. Path towards **imine-II.** Energies are in kcal mol^{-1}, distances in Å, and Wiberg indexes are in parentheses.

3. Experimental Section

3.1. Reagents and Equipment

The reactions were carried out under an Argon atmosphere, employing oven-dried glassware. Deuterated acetic acid (AcO*d*$_4$) was purchased from Aldrich. $^{13}CH_2O$ and $^{15}NH_4Cl$ were acquired to Santa Cruz and used as received.

The ^{1}H and ^{13}C NMR spectra were acquired at 300.13 and 75.48 MHz respectively, on a Bruker Avance 300 spectrometer. The resonance of C*H*$_3$COH in AcO*d*$_4$ (δ= 2.07 ppm) was used as an internal standard. Chemical shifts are reported in parts per million in the δ scale and the magnitudes of the coupling constants (J) are given in Hertz.

The temperature ramp experiments were carried out with a Bruker Avance III 400 MHz spectrometer (400.13 MHz for ^{1}H, 100.61 MHz for ^{13}C).

The ^{15}N-^{1}H HMBC experiments were carried out in a Bruker 700 MHz NMR spectrometer equipped with an Avance III console and a TXI probe (700.2 MHz for ^{1}H, 176.07 MHz for ^{13}C and 70.95 MHz for ^{15}N).

3.2. Experimental Procedure

3.2.1. Synthesis of $^{13}C^{15}N$-Hexamethylenetetramine ($^{13}C_6H_{12}{}^{15}N_4$)

Labelled ammonia, obtained by heating $^{15}NH_4Cl$ (258.32, 4.83 mmol) with $CaCl_2$ was bubbled into a beaker containing a solution of $^{13}CH_2O$ (750 uL of a 20% wt. solution of $^{13}CH_2O$ in water, 4.83 mmol). The temperature of the solution was kept below 20 °C with an ice-bath. When the bubbling stopped, the solution was maintained for 20 min at this temperature. Then, the beaker was heated in a hot plate, removing the water until constant weight. With this procedure, 84.64 mg (0.6038 mmol, 75% yield) of $^{13}C^{15}N$-hexamethylenetetramine was obtained as a white solid. ^{1}H NMR (AcO*d*$_4$): δ = 4.92 ppm (s); ^{13}C NMR: δ = 71.6 ppm; ^{15}N NMR: δ = 39.5 ppm.

3.2.2. Temperature Ramp Experiment for HMTA

In an NMR tube, HMTA (50 mg, 0.357 mmol) was dissolved in AcO*d*$_4$ (0.5 mL). The tube was placed in the NMR apparatus and the ^{1}H NMR spectrum of the sample was acquired every 10 K from

298 K until 363 K. When signal changes were evident, ^{1}H-^{13}C-HSQC, ^{1}H-^{13}C-HMBC, ^{1}H-^{1}H-COSY, and NOESY spectra were concomitantly acquired.

At 363 K, ^{1}H NMR spectra were acquired every 3 minutes for 90 min. At the end, 2D NMR spectra were also acquired, and then the probe was cooled until room temperature. At this point, additional ^{1}H NMR, ^{13}C NMR, and 2D spectra were acquired.

3.2.3. NMR Spectra Acquisition for ^{13}C-^{15}N-HMTA

In an NMR tube, ^{13}C-^{15}N-HMTA (50 mg, 0.357 mmol) was dissolved in AcOd_4 (0.5 mL). The ^{1}H NMR, ^{1}H-^{13}C-HSQC, and ^{1}H-^{15}N-HMBC spectra were acquired at 298 K, and then, the temperature was raised until 343 K with 10 K intervals. An ^{1}H-NMR spectrum was acquired in each interval. At 343 K, complimentary ^{1}H NMR, ^{1}H-^{13}C-HSQC, and ^{1}H-^{15}N-HMBC spectra were obtained.

4. Conclusions

We have used a combined analysis of ^{1}H, ^{13}C and ^{15}N NMR data of HMTA in AcOH-d_4 under variable temperature conditions with chemometrics tools to demonstrate that HMTA undergoes sequential solvent-mediated protonation, followed by ring-opening to give a Mannich base intermediate (**imine-I**) and a further and unexpected [1,5-H]-shift to afford compound **imine-II** as a stable product. The mechanism proposed for the formation of **imine-II** is fully supported by theoretical studies. These findings add to current knowledge of the stability of HMTA and may explain some of the problems associated with the use of HMTA as Mannich bases in multiple applications with poorly active substrates and prolonged reaction times.

Acknowledgments: The authors gratefully acknowledge Consejo Nacional de Investigaciones Científicas y Técnicas (CONICET), Agencia Nacional de Promoción Científica y Tecnológica (ANPCyT), Agencia Santafesina de Ciencia, Tecnología e Innovación (ASACTeI, institutional grant AC 2015-0005), and Alexander von Humboldt Foundation.

References

1. (a) Hajji, M.; Amiri, N.; Ben Taheur, F.; Bujacz, A.; Nasri, H.; Guerfel, T. *Solid State Sci.* **2020**, *100*, 106117; (b) Wang, G.; Yue, H.; Xu, Y.; Liu, G.; Jin, R.; Gao, S.J. *Coll. Interf. Sci.* **2020**, *570*, 332; (c) Wang, C.; Li, Z.; Wu, K.; Liu, J.; Yang, X.; Kong, X.; Huang, Y.; Wang, W.; Yang, Y. *Biomass Bioen.* **2020**, *133*, 105448.
2. (a) Liu, S.; Zhou, J.; Song, H. *Adv. Energy Mater.* **2018**, *8*, 1; (b) Kirillov, A.M. *Coord. Chem. Rev.* **2011**, *255*, 1603.
3. (a) Dou, X.; Li, G.; Zhang, W.; Lu, F.; Luo, D.; Liu, W.; Yu, A.; Chen, Z.J. *Mater. Chem. A* **2020**, *8*, 5062; (b) Kim, K.H.; Motoyama, S.; Abe, Y.; Kawamura, M.; Kiba, T. *Mater. Lett.* **2019**, *254*, 154.
4. (a) Javanbakht, F.; Razavi, B.; Salami-Kalajahi, M.; Roghani-Mamaqani, H.; Ommati, M. *Polym. Adv. Technol.* **2020**, *31*, 226; (b) Lei, Z.; Ji, J.; Wu, Q.; Zhang, J.; Wang, Y.; Jing, X.; Liu, Y. *Polymer* **2019**, *178*, 121587.
5. (a) Abeyrathna, N.; Washington, K.; Bashur, C.; Liao, Y. *Org. Biomol. Chem.* **2017**, *15*, 8692; (b) Ayudhya, T.I.; Raymond, C.C.; Dingra, N.N. *Dalton Trans.* **2017**, *46*, 882.
6. (a) Vinogradoff, V.; Fray, N.; Duvernay, F.; Briani, G.; Danger, G.; Cottin, H.; Theulé, P.; Chiavassa, T. *Astron. Astrophys.* **2013**, *551*; (b) Vinogradoff, V.; Rimola, A.; Duvernay, F.; Danger, G.; Theulé, P.; Chiavassa, T. *Phys. Chem. Chem. Phys.* **2012**, *14*, 12309.
7. (a) Hrdina, R.; *Synth.* **2019**, *51*, 629; (b) Bin Yang, H.; Feceu, A.; Martin, D.B.C. *ACS Catal.* **2019**, *9*, 5708.
8. (a) Cai, H.; Li, Z.; Huang, C.W.; Park, R.; Shahinian, A.H.; Conti, P.S. *Nucl. Med. Biol.* **2010**, *37*, 57; (b) Ma, L.; Meng, L.; Wang, Y.; Wu, G.; Fan, D.; Yu, J.; Qi, M.; Huang, Y. *RSC Adv.* **2014**, *4*, 39156.
9. (a) Masurier, N.; Moreau, E.; Lartigue, C.; Gaumet, V.; Chezal, J.-M.; Heitz, A.; Teulade, J.-C.; Chavignon, O.J. *Org. Chem.* **2008**, *73*, 5989; (b) Chavan, S.P.; Lasonkar, P.B. *Tetrahedron Lett.* **2013**, *54*, 4789.
10. (a) Mathew, T.; Papp, A.; Paknia, F.; Fustero, S.; Surya Prakash, G.K. *Chem. Soc. Rev.* **2017**, *46*, 3060; (b) Singh, B. *Synlett* 2011, 2903.
11. (a) Heravi, M.M.; Abdolhosseini, N.; Oskooie, H.A. *Tetrahedron Lett.* **2005**, *46*, 8959; (b) Teimouri, M.B.; Mivehchi, H. *Synth. Commun.* **2005**, *35*, 1835.
12. (a) Cahiez, G.; Duplais, C.; Moyeux, A. *Org. Lett.* **2007**, *9*, 3253; (b) Yan, Y.; Sun, S.; Cheng, J.J. *Org. Chem.* **2017**, *82*, 12888.

13. (a) Ranatunga, S.; Tang, C.-H.A.; Kang, C.W.; Kriss, C.L.; Kloppenburg, B.J.; Hu, C.-C.A.; Del Valle, J.R.J. *Med. Chem.* **2014**, *57*, 4289; (b) Affeldt, R.F.; De Amorim Borges, A.C.; Russowsky, D.; Severo Rodembusch, F. *New J. Chem.* **2014**, *38*, 4607.
14. (a) He, H.; Wang, Y.; Zhang, J.J. *Disp. Sci. Technol.* **2015**, *36*, 626; (b) Li, H.; Zhai, Z.; Xin, B.J. *Chem. Res.* **2015**, *39*, 238.
15. We arrive to this conclusion because the mass balance according to the abundance of the signals remains constant along the experiment.
16. (a) Rivera, A.; Sadat-Bernal, J.; Ríos-Motta, J.; Bolte, M. *Crystals* **2019**, *9*, 520. (b) Mahmoud, M.M.; Wallwork, S.C. *Acta Cryst.* **1979**, *B35*, 2370.
17. Chen, S.-P.; Wang, C.-F.; Zhou, H.-T.; Tan, Y.-H.; Wen, H.-R.; Tang, Y.-Z. *Chem. Phys. Lett.* **2019**, *715*, 45.
18. (a) Lemmerer, A.; Motlaung, X. *Acta Cryst.* 2017, *E73*, 1630; (b) Goloveshkin, A.S.; Lenenko, N.D.; Korlyukov, A.A.; Golub, A.S. *ACS Omega* **2020**, *5*, 4603.
19. Rivera, A.; Pacheco, D.J.; Ríos-Motta, J.; Fejfarová, K.; Dušek, M. *Tetrahedron Lett.* **2012**, *53*, 6132.
20. (a) Wang, L.; Xiao, J. *Adv. Synth. Catal.* **2014**, *356*, 1137; (b) Huang, Y.W.; Frontier, A.J. *Org. Lett.* **2016**, *18*, 4896.